Ocean Modelling 83 (2014) 1–10

Contents lists available at ScienceDirect

Ocean Modelling

journal homepage: www.elsevier.com/locate/ocemod

Energetics and mixing efficiency of lock-exchange flow

Mehmet Ilıcak

Uni Climate, Uni Research AS, and Bjerknes Centre for Climate Research, Allégaten 55, 5007 Bergen, Norway

ARTICLE INFO

Article history:
Received 29 August 2013
Received in revised form 8 August 2014
Accepted 13 August 2014
Available online 28 August 2014

Keywords:
Lock-exchange flow
Mixing efficiency
Mixing
Background potential energy

ABSTRACT

Mixing efficiency between different water masses is typically assumed to be constant in diapycnal mixing parameterizations used in ocean models. As of now, most coarse resolution ocean circulation models employ a constant mixing efficiency value of 0.2 for the shear driven mixing, internal waves and bottom boundary layer parameterizations. This study investigates the energetics and mixing efficiency of the lock-exchange flow at different Reynolds numbers. The lock-exchange experiment resolves Kelvin–Helmholtz vortices and is an idealized test case for oceanic gravity currents. At first, the required spatial resolution for the direct numerical simulations (DNS) is determined in simulations at a constant Reynolds number of 3500. The evolution of background potential energy and tracer variance are used to assess model results. We found that the model spatial resolution should resolve at least the Kolmogorov scale but not necessarily the Batchelor scale if convergences of background potential energy, tracer variance and dissipation are considered. Simulations at Reynolds number of 125, 500, 1000, 2500, 3500, 5000, 6000, 10,000 show that the mixing efficiency in the lock-exchange flow is smaller than 0.2, and it saturates around 0.12 when Reynolds numbers exceed the value of 2500.

1. Introduction

Mixing is an irreversible process in which energy is extracted from the mean flow through vertical shear production and destabilizing buoyancy flux (Cushman-Roisin and Beckers, 2011). Turbulent mixing of water masses of different densities is an important process for both coastal and large-scale ocean circulation. Near oceanic coasts, mixing is an important consequence of the breaking of internal waves (Klymak et al., 2012). In the deep oceans, vertical stratification is maintained by irreversible mixing (Munk, 1966). The total amounts of mixing and available potential energy required to mix oceanic water masses are poorly known in the ocean. Only some estimates are available (Wunsch and Ferrari, 2004). A fundamental parameter needed to estimate mixing is the mixing efficiency coefficient. One possible definition of mixing efficiency is the ratio of irreversible mixing to the sum of irreversible mixing and kinetic energy dissipation (Peltier and Caulfield, 2003). The potential energy increase due to mixing processes is in fact bounded by the product of power input (i.e. winds and tides) and the mixing efficiency coefficient (Wunsch and Ferrari, 2004).

Mixing efficiency values are currently debated. One line of thought assumes that the mixing efficiency in turbulent flows is approximately constant at 0.2 (Osborn, 1980; Peters et al., 1995) with a definition of ratio of buoyancy flux to turbulent energy dissipation rate. Although this quantity has been used extensively by the oceanography community to compute mixing in the ocean (Gregg and Ozsoy, 2002; Peters and Johns, 2005), it conflicts with the historical definition of efficiency as pointed out by Moum (1996). The definition of "flux coefficient" (Γ) term by Osborn (1980) might be more appropriate to use instead of mixing efficiency. One can compute the mixing efficiency from flux coefficient as $\mu = \Gamma/(1+\Gamma) \approx 0.166$. Nevertheless the assumption of constant 0.2 mixing efficiency is consistent with the traditional view on the ocean circulation as described in the following. Sandström (1908) postulated that an overturning circulation cannot be maintained in a closed domain if the buoyancy sources and sinks are at the same geopotential level. This has fundamental implications for ocean circulation since the ocean is both cooled and heated at the surface (i.e. horizontal convection) (Ilıcak and Vallis, 2012). After Sandström's experiments, it was concluded that the ocean cannot sustain a meridional overturning circulation (MOC) if forced by buoyancy alone. An additional mechanical forcing is required to maintain the MOC. Energy inputs from surface winds and tides are the main candidates for this. Wunsch and Ferrari (2004) estimated that 2 TW of mechanical energy is required to maintain the MOC and that 1.5 TW of the total energy is coming from internal tides. Most climate models employ internal tides and bottom boundary layer parameterizations using the constant

E-mail address: mehmet.ilicak@uni.no

http://dx.doi.org/10.1016/j.ocemod.2014.08.003
1463-5003/

mixing efficiency of 0.2 (Simmons et al., 2004; Legg et al., 2006; Dunne et al., 2012).

Another line of thought puts the 0.2 value under discussion. Recent three-dimensional (3D) direct numerical simulations (DNS) show that horizontal convection can have strong overturning and be highly efficient (Scotti and White, 2011). As a result, mixing efficiency values between 0.8 and 0.9 are estimated (Scotti and White, 2011; Gayen et al., 2013). These values necessitate a change in our understanding of the ocean energy budget. If buoyancy forcing at the surface can be responsible for strong overturning and the sinking regions are so efficient, this means that the overall contribution of the other mechanical forcing mechanisms might be overestimated in the traditional view.

There is more evidence which disagrees with the traditional assumption of mixing efficiency being equal 0.2. Laboratory experiments of two-layer exchange flows spanned a wide range of Reynolds numbers (Re) up to 220,000 showed that the efficiency of mixing saturates with a value around 0.11 for Re > 50,000 (Prastowo et al., 2008; Prastowo et al., 2009). Laboratory internal-wave breaking experiments found that mixing efficiency is between 0.03 and 0.08 for waves of varied incident amplitudes (Hult et al., 2011). There is also a wide spread of mixing efficiency values in observations. Ruddick et al. (1997) found that mixing efficiency decreases systematically with increasing density ratio and increases systematically with increasing buoyancy Reynolds number in the North Atlantic Central Water. They also described previous values of efficiency of mixing from a variety of locations by other observers (see their Table 2). These mixing efficiency values are ranging from 0 to 0.4 (Ruddick et al., 1997). In the numerical simulations of Caulfield and Peltier (2000) and Peltier and Caulfield (2003), the evolution of a Kelvin–Helmholtz roll during a transition from a 2D symmetric laminar flow to a fully 3D turbulent state is investigated. The simulations show that the instantaneous mixing efficiency is much larger than 0.2, but it decreases with time and the average mixing efficiency approaches a value of 0.15. In similar simulations, Mashayek and Peltier (2011) found that the time-averaged efficiency increases with increasing Re and the mixing efficiency reaches values as large as 0.5. In addition, Mashayek et al. (2013) employed direct numerical simulations of shear-induced turbulence in stably stratified free shear flow. They also showed that constant 0.2 mixing efficiency fails at higher Richardson numbers provided that the Reynolds number is sufficiently high. Smyth et al. (2001) investigated the time evolution of mixing in turbulent overturns using both numerical simulations and microstructure profiles obtained during field experiments. They showed that mixing efficiency can change by more than an order of magnitude over the life of a turbulent overturn. Pham and Sarkar (2010) investigated the interaction between an unstable shear layer and a stably stratified jet showing that mixing efficiency exceeds 0.2, especially in highly turbulent areas.

The aim of this study is to investigate the mixing efficiency values in idealized gravity current simulations. A number of 3D direct numerical simulations of lock-exchange flow are performed. Such a choice is justified by the fact that the lock-exchange experiment is highly relevant to gravity currents, overflows (Ilıcak et al., 2008) and exchange flows in the ocean (Ilıcak et al., 2009; Ilıcak and Armi, 2010). In each of these shear- and buoyancy-driven flows, mixing occurs through Kelvin–Helmholtz instabilities. The advantage of the 3D lock-exchange problem is that it contains different turbulent processes such as shear-driven mixing, internal waves and gravitationally-unstable phases in an enclosed domain (Özgökmen et al., 2009). The effect of Reynolds number on the mixing efficiency is investigated. Different simulations are conducted spanning a wide range of Re from 125 and to 10,000. Mixing of the density field is quantified using the background potential energy (Winters et al., 1995). Results indicate that the mixing increases (i.e. background potential energy increases) as the Reynolds number increases. For the low and moderate Reynolds numbers, the mixing increases monotonically. At Re = 2500, the mixing efficiency saturates at around 0.12. All mixing efficiency values are, however, consistently lower than 0.2.

The paper is organized as follows: In Section 2, the numerical model and the parameters of all numerical simulations are described. Results for the lock-exchange problem are presented in Section 3. Finally, major findings are summarized in Section 4.

2. Model description and numerical setup

In this study, the non-hydrostatic version of MIT general circulation model (MITgcm) is used with the Boussinesq approximation. The MITgcm is a three dimensional C-grid fully incompressible Navier Stokes equations model (Marshall et al., 1997). The non-dimensional model governing equations are

$$\frac{D\mathbf{u_i}}{Dt} = -\frac{\partial p}{\partial x_\mathbf{i}} - Ri_0\rho'\delta_{i3} + \frac{1}{\mathrm{Re}}\frac{\partial^2 \mathbf{u_i}}{\partial x_j^2}, \tag{1}$$

$$\frac{\partial \mathbf{u}_j}{\partial x_j} = 0, \tag{2}$$

$$\frac{D\rho'}{Dt} = \frac{1}{\mathrm{RePr}}\frac{\partial^2 \rho'}{\partial x_j^2}, \tag{3}$$

where $\mathbf{u}$ is the three dimensional velocity, p is the pressure, ρ' is the density perturbation and D/Dt is the material derivative. The non-dimensionalization is performed using a characteristic velocity (U_0), a characteristic length scale (l_0), a characteristic time scale ($\tau^* = l_0/U_0$), density difference ($\Delta\rho'$) and pressure $\rho_0 U_0^2$ for $\mathbf{u}$, x, ρ', and p respectively. The initial Reynolds number ($Re = U_0 l_0/\nu$) expresses the relative importance of viscous effects where ν is the molecular viscosity. The bulk Richardson number ($Ri_0 = g\Delta\rho' 0.5H/(\rho_0 \Delta U_0^2)$) indicates the importance of stratification and shear. Finally, the Prandtl number is defined as $\mathrm{Pr} = \nu/\kappa$, where κ is the molecular diffusivity.

The non-dimensional computational domain is $0 \leqslant x \leq 8$, $0 \leqslant y \leqslant 1/2$ and $0 \leqslant z \leqslant 1$ since vertical depth is used as the characteristic length scale, $H = l_0$. At all boundaries, no-flow and free-slip boundary conditions are used for the velocity components, while no-flux conditions are used for the density perturbation ρ'. The lock-exchange problem is initialized with dense fluid on the left separated from the light fluid on the right

Table 1
Numerical simulations setup and mixing efficiency values for Re = 3500. To resolve the Kolmogorov scale 94.2 million grid points are required.

Re = 3500	# of grid points in x, y, z	Grid resolution (Δ)	Total # of points (N^3)	Mixing efficiency
Exp1	$576 \times 36 \times 72$	$\Delta = 1.38 \times 10^{-2}$	≈ 1.5 million	0.1312
Exp2	$1152 \times 72 \times 144$	$\Delta = 6.94 \times 10^{-3}$	≈ 12 million	0.1019
Exp3	$2304 \times 144 \times 288$	$\Delta = 3.47 \times 10^{-3}$	≈ 95 million	0.0956
Exp4	$3456 \times 216 \times 432$	$\Delta = 2.31 \times 10^{-3}$	≈ 322 million	0.0955

Table 2
Reynolds number vs. number of grid points for the lock-exchange problem. The last column shows required DNS grid points according to Pope (2000).

Re	# of grid points in *x*, *y*, *z*	Total number of points (N^3)	$Re^{9/4}$
125	$1152 \times 72 \times 144$	≈ 12 million	≈ 52000
500	$1152 \times 72 \times 144$	≈ 12 million	≈ 1.1 million
1000	$1152 \times 72 \times 144$	≈ 12 million	≈ 5.6 million
2500	$2304 \times 144 \times 288$	≈ 95 million	≈ 47 million
3500	$2304 \times 144 \times 288$	≈ 95 million	≈ 94 million
5000	$3456 \times 216 \times 432$	≈ 322 million	≈ 210 million
6000	$3456 \times 216 \times 432$	≈ 322 million	≈ 316 million
10,000	$7680 \times 480 \times 960$	≈ 3.5 billion	1 billion

by a sharp interface with a sinusoidal perturbation in the *y*-direction with an amplitude of 0.125 to induce 3D turbulence. Adjustment occurs in which lighter water moves above heavier water. The Kelvin–Helmholtz (KH) rolls are observed due to the shear between two layer exchange flow. The mixing takes place by KH rolls stirring towards smaller scale, and their turbulent breakdown due to secondary instabilities in the cross-direction (Özgökmen et al., 2009). In the lock-exchange problem, the characteristic velocity is the frontal speed of the gravity current which has an analytical form of $U_0 \approx 0.5\sqrt{g\Delta\rho' H/\rho_0}$ in the inviscid limit (Benjamin, 1968). Thus, the bulk Richardson number is set to $Ri_0 = 2$. The Prandtl number is set to 7 in all cases since the density is a function of temperature only. All simulations were run for around ten gravity current travel times (i.e. $10l_0/U_0$) along the length of the box.

Direct numerical simulations of the governing equations are employed to ensure that all scales of motion are resolved including the Kolmogorov length scale, $\lambda_K = \left(\frac{\nu^3}{\varepsilon}\right)^{1/4}$ where $\varepsilon = 2\nu S_{ij}S_{ij}$ is the kinetic energy dissipation rate and $S_{ij} = \frac{1}{2}\left(\frac{\partial u_i}{\partial x_j} + \frac{\partial u_j}{\partial x_i}\right)$ is the strain rate tensor. Pope (2000) describes that the necessary number of grid points (N) in direct numerical simulations are proportional to $Re^{9/4}$ for homogeneous turbulence. However, in stratified turbulence the Batchelor scale, $\lambda_B = \lambda_K/Pr^{1/2}$, should also be resolved. Resolving the Batchelor scale is crucial for some small scale processes such as double diffusion (i.e. salt fingers) where different molecular diffusion coefficients of salinity and temperature induce molecular scale mixing. In the next section, effects of resolution on the mixing are investigated for a constant Reynolds number. The appropriate spatial resolutions that resolve energetics at all length scales will be chosen accordingly. We will show that resolving the Batchelor scale is not necessary for the diagnostics considered.

To quantify the dynamic regimes of the evolving flow fields, time dependence of volume averaged energy terms are computed. The potential energy (PE) and kinetic energy (KE) are computed using $PE = g\int_V \rho z dV$ and $KE = \int_V (u^2 + v^2 + w^2)dV$. Mixing between water masses of different density is an irreversible process which leads to an increase in the center of gravity. Changes in the mixing are accurately computed by tracking changes in the background potential energy, BPE (Winters et al., 1995). The BPE is a single global number that reflects the effect of diapycnal mixing in a closed system (Ilıcak et al., 2012). BPE is the minimum potential energy obtained by sorting the density without mixing. To compute the BPE, all water parcels are sorted, with the heaviest parcels at the bottom and lighter parcels above. The sorting results in a redistribution of the parcels throughout the model domain and a sorted density state ρ^*. The reference potential energy is then calculated as the volume integral of the density-weighted geopotential:

$$BPE = g\iiint \rho^* z dV. \tag{4}$$

The available potential energy, which might be converted into KE, is simply defined as $APE = PE - BPE$, whereas the total energy is defined as $TE = PE + KE$. A brief summary of evolution equations of different energy terms is discussed in the following. The potential energy equation may be written as (Caulfield and Peltier, 2000)

$$\frac{dPE}{dt} = Ri_0\rho w + \mathscr{D}_\rho \tag{5}$$

where $\mathscr{D}_\rho = Ri_0(\rho_{bottom} - \rho_{top})/(H\mathrm{RePr})$ is the positive definite molecular diapycnal mixing due to molecular diffusion down the mean vertical gradient, and represents a conversion of internal energy to background potential energy. $Ri_0\rho w$ is the conversion term between potential and kinetic energy. Following Caulfield and Peltier (2000), the governing equations for BPE, APE and KE are

$$\frac{dBPE}{dt} = \mathscr{M} + \mathscr{D}_\rho, \tag{6}$$

$$\frac{dAPE}{dt} = Ri_0\rho w - \mathscr{M}, \tag{7}$$

$$\frac{dKE}{dt} = -Ri_0\rho w - \varepsilon \tag{8}$$

where $\mathscr{M}$ is the irreversible mixing rate and ε is the kinetic energy dissipation rate. The mixing efficiency (μ) can be defined in different ways. A common definition of μ is the ratio of irreversible mixing (the increase in background potential energy of the density field) to the sum of the irreversible mixing and the kinetic energy dissipation (Peltier and Caulfield, 2003). Thus, mixing efficiency can be defined as the following

$$\mu_1 = \frac{\int_0^t \mathscr{M}(\tau)d\tau}{\int_0^t \mathscr{M}(\tau)d\tau + \int_0^t \varepsilon(\tau)d\tau} \tag{9}$$

and by definition it is always smaller than one. Note that, the definition of mixing efficiency used here is different from the one defined by Osborn (1980). He defined a mixing efficiency function $\Gamma = R_f/(1 + R_f)$ where R_f is the flux Richardson number. Since a Boussinesq model with linear equation of state is used in this study, we do not account for effects of non-linear equation of state on mixing efficiency discussed by Tailleux (2009).

3. Results

3.1. Effects of resolution on mixing

In this section, the resolution suitable for simulations involving different Reynolds numbers is addressed. Four simulations with different spatial resolutions at a constant Reynolds number of 3500 are conducted. The horizontal and vertical resolutions employed here can be found in Table 1. Hartel et al. (1997) argued that the model resolution should be related to $\Delta \approx (\mathrm{RePr})^{-1/2}$ for the DNS lock-exchange simulations. For Re = 3500 and Pr = 7, that leads to $\Delta = 6.388 \times 10^{-3}$ which is similar to the Exp2 in Table 1. Note that the Kolmogorov dissipation scale is resolved (i.e. $N^3 \sim Re^{9/4}$) starting from the third simulation (Exp3). Cross sectional snapshots of the density field for different resolutions are shown in Fig. 1. Kelvin–Helmholtz (KH) rolls are observed in all cases. Density gradients sharpen with increased resolution. Two vertical eddies (i.e. Kelvin–Helmholtz billows) break at $x = 3$ and $x = 5$ for the first time since the beginning of simulations. The locations of KH rolls coincide in each of the simulations. The formation of new water masses (light green and yellow) is due to irreversible mixing. In the coarsest resolution case (Exp1), mixing is largest.

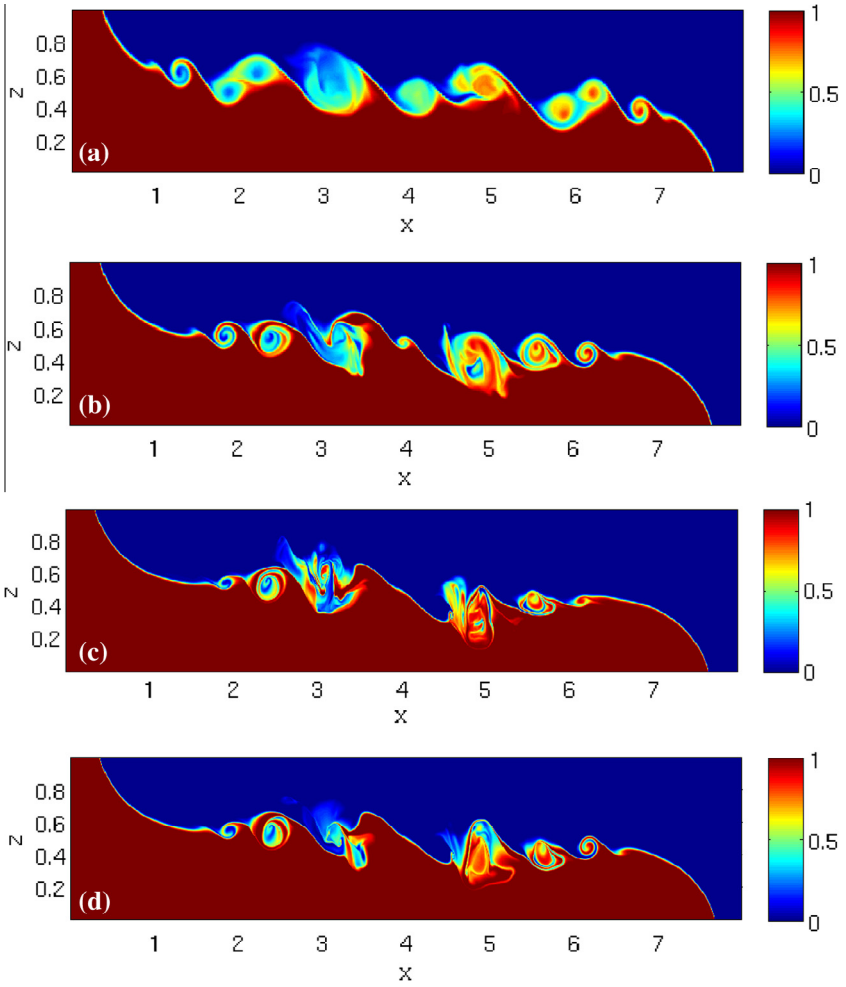

Fig. 1. Snapshots of density field for Re = 3500 at $y = 0.25$ using different resolutions; (a) $\Delta x = 0.0138$, (b) $\Delta x = 6.94 \times 10^{-3}$, (c) $\Delta x = 3.47 \times 10^{-3}$, *(d)* $\Delta x = 2.31 \times 10^{-3}$.

This qualitative argument will be quantified later using the evolution of the background potential energy. The logarithm of kinetic energy dissipation ($log_{10}\varepsilon$) is shown in Fig. 2 for different resolutions. The non-dimensional magnitude of ε is on the order of 10^{-7} for Exp1 and of 10^{-8} for Exp2 simulations in high shear regions. Exp3 and Exp4 cases have similar ε fields with magnitude of $O(10^{-9})$, where most of the dissipation is associated with breaking of KH eddies ($x = 3$ and $x = 5$). Once again, high values of dissipation rate indicate that the largest amount of mixing takes place in Exp1. There are two reasons behind this. The first one is energy exchanges occurring through buoyancy flux, viscous dissipation or diabatic mixing (Winters et al., 1995). Increased viscous dissipation leads to an increased internal energy which contributes to an increase in background potential energy through irreversible mixing (Hughes et al., 2009). The second reason is spurious mixing. Under resolved shear regions induce a large amount of numerical mixing.

Fig. 3(a) presents the time evolution of the total energy, potential energy kinetic energy, background potential energy and available potential energy in Exp3. There are cyclic conversions between KE, PE and APE due to the fluid motion in this enclosed domain, whereas BPE increases monotonically due to irreversible mixing and total energy (TE) decreases due to mixing and dissipation. Note that the energy terms are normalized by the initial total energy which is equal to the initial PE since the fluid is at rest at $t/\tau^* = 0$. The energetics shown here are consistent with those described in Özgökmen et al. (2009) (see their Fig. 3) who performed 3D DNS simulations with a high order spectral element model. Fig. 3(b) shows the comparison between the KE time derivative and the sum of momentum dissipation and buoyancy conversion terms. It is clear that energy equations are balanced in the simulations as the two curves coincide at all times. This is important to ensure and check that all scales of motions are resolved.

Fig. 4(a) depicts the evolution of relative background potential energy (RBPE) over time for different spatial resolutions. Relative background potential energy is defined as

$$RBPE(t) = \frac{BPE(t) - BPE(t=0)}{BPE(t=0)} \tag{10}$$

which shows the relative increase of the BPE with respect to the initial state as a result of mixing. During the integration period, RBPE increases monotonically due to irreversible mixing. The RBPE curves from the Exp3 and Exp4 are similar (blue and black lines) which is a clear indication of numerical convergence for the RBPE metric. Since the grid Reynolds number exceeds 2 in Exp1, RBPE is larger because of spurious numerical mixing (Ilıcak et al., 2012). The maximum RBPE value reached 0.11 at $t/\tau^* = 10$. This is almost 55% larger than the highest resolution simulation Exp4 (blue line). Özgökmen et al. (2009) also found increased mixing in a coarse resolution simulation in their 3D dam-breaking case. Fig. 4(b) shows time evolution of the tracer variance (χ) for different simulations. The tracer variance (or dissipation) term can be derived by

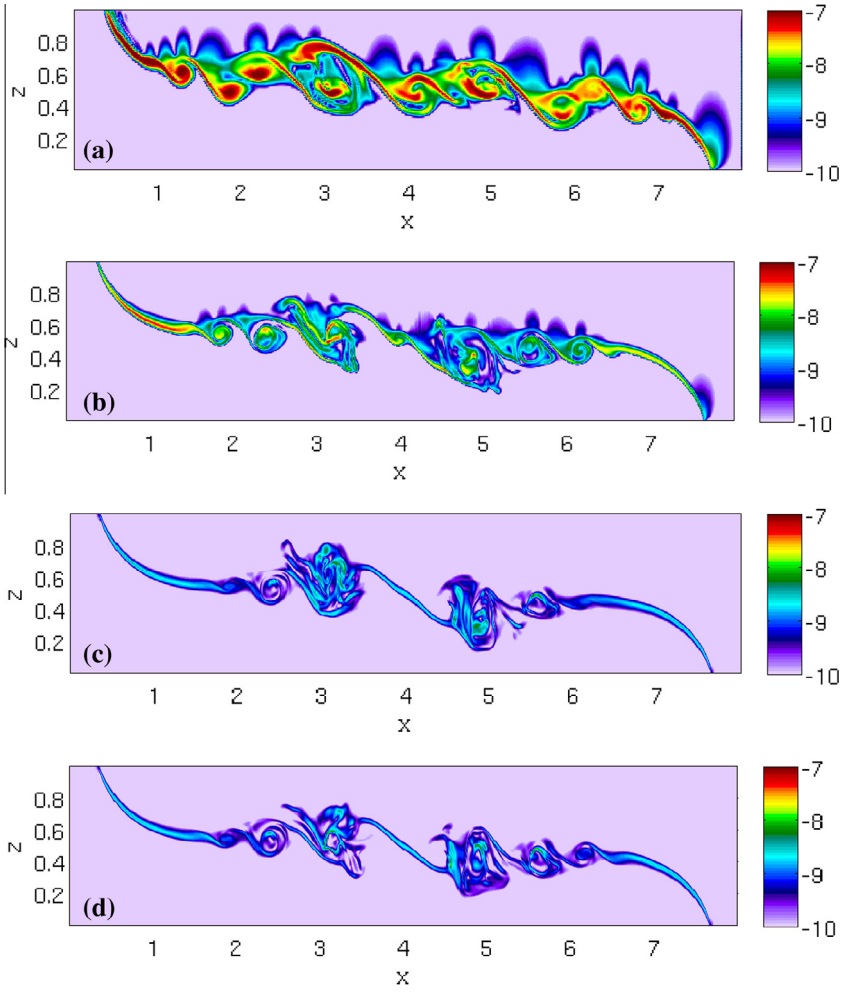

Fig. 2. Snapshots of logarithmic kinetic energy dissipation field (ε) for Re = 3500 at $y = 0.25$ using different resolutions; (a) $\Delta x = 0.0138$, (b) $\Delta x = 6.94 \times 10^{-3}$, (c) $\Delta x = 3.47 \times 10^{-3}$, (d) $\Delta x = 2.31 \times 10^{-3}$.

multiplying Eq. (3) by ρ' (Winters and Young, 2009; Ilıcak and Vallis, 2012) and expressed in a closed system as

$$\chi = \frac{|\nabla \rho'|^2}{\mathrm{RePr}}. \tag{11}$$

The peaks in Fig. 4(b) indicate that tracer dissipates vigorously. There is an early peak in χ for the coarse resolution simulations. There is an offset between high amount of mixing and the peak of the tracer variance in all simulations. For the coarse resolution the main peak is observed before $t/\tau = 2$ while the BPE keeps increasing. For the high resolution cases the main peak is of smaller amplitude and lags behind the main peak of coarse resolution cases. The local peaks of high-resolution simulations remain smaller in amplitude until $t/\tau = 6$, but become larger later on. We believe that it is due to spurious numerical mixing in coarse-resolution runs before $t/\tau = 6$. This mixing removes the energy from the system, so that the peaks become smaller afterwards. Once again, evolution of tracer variance in high resolution simulations is similar to each other. Finally, mixing efficiency values are computed for different simulations. For Exp1, mixing efficiency is around $\mu = 0.1312$ which is much higher than the mixing efficiencies for the other cases. For Exp3 and Exp4, μ converges to a value of 0.0956 (Table 1). Note that since the dissipation is higher in the coarse resolution case, the efficiency is large due to high amount of irreversible mixing.

In summary, changing spatial resolution provides us with insight as to which resolution is required for DNS. Our results indicate that models with resolution coarser than the Kolmogorov scale overestimate mixing and tracer variance. Numerical simulations resolving down to the Kolmogorov scales are sufficient for DNS in terms of evolution of RBPE, ε and χ metrics. Thus, DNS resolving the Kolmogorov scale are conducted in the next section.

3.2. Simulations with increasing Reynolds number

In this section, eight different Reynolds numbers simulations are conducted for the lock-exchange problem. The number of grid points for the corresponding Re are given in Table 2. Total number of grid points in all simulations are larger than the number of grid points suggested by Pope (2000) to perform DNS. All simulations are integrated until a non-dimensional time of $t/\tau^* = 10$ where $\tau^* = L/U_0$ is the advection time scale.

Fig. 5 shows a cross section of the density fields in the middle of the domain by the time the counterpart gravity currents reach the side walls at different Reynolds numbers. The flow is laminar in the Re = 125 and Re = 500 cases. Two KH rolls are visible in the Re = 1000 simulation. As Re is increased, KH rolls become more distinct, e.g, at Re = 2500 and Re = 3500. The initial 2D KH rolls break down due to a 3D convective instability (Klaassen and Peltier, 1991), in which the stream-wise vortices stretch and tilt the span-wise vorticity concentrated in KH rolls (Özgökmen

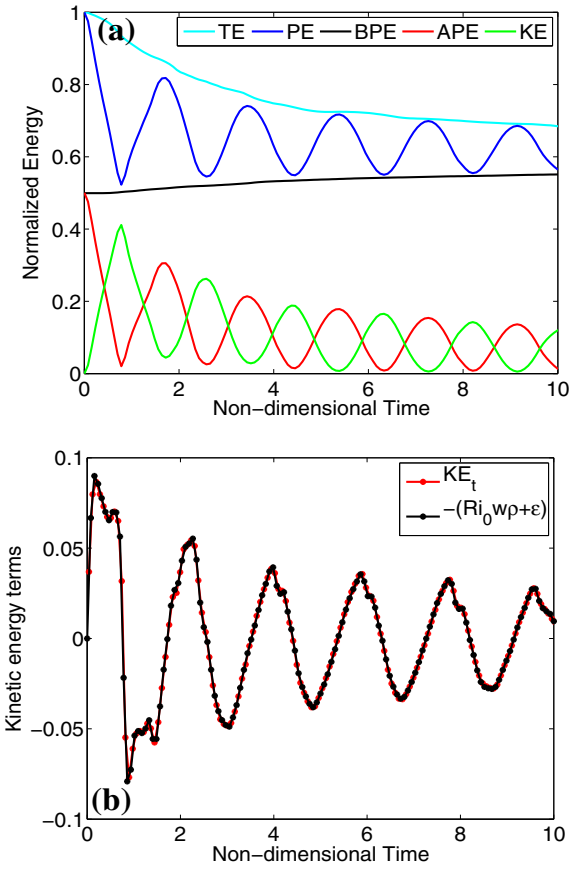

Fig. 3. Time evolution of (a) the energy terms (TE = total energy, PE = potential energy, BPE = background potential energy, APE = available potential energy, KE = kinetic energy) for Exp3, and (b) the terms in the KE equation for Exp3 (see Eq. (8)). Energy budget is also closed in other simulations (not shown).

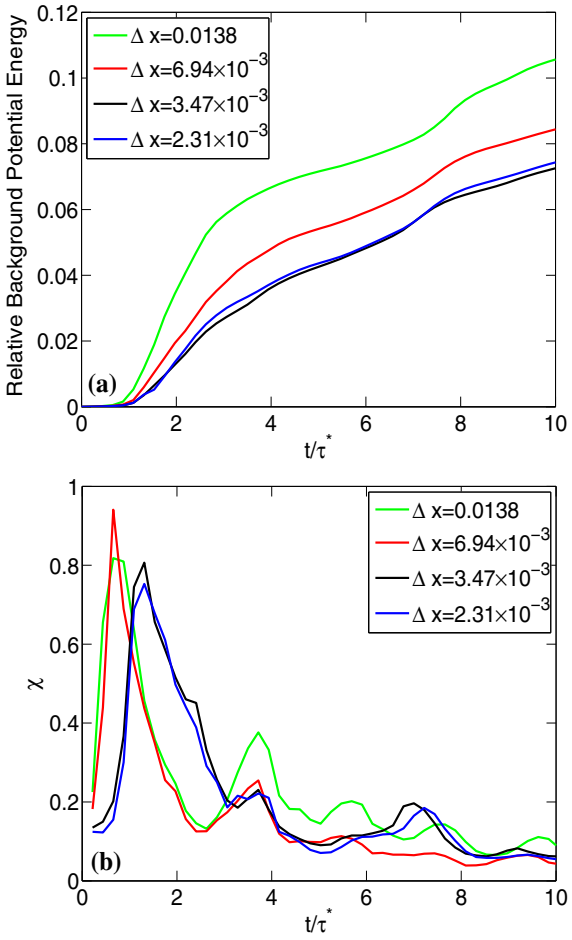

Fig. 4. Time evolution of (a) relative background potential energy and (b) tracer variance for Re = 3500 using different spatial resolutions indicated in the legend.

et al., 2009). There are more rapid developments of 3D flow structures, and secondary instabilities started to destroy the KH overturns for the first time at around $x \approx 3.2$ and $x \approx 5.1$ in higher Reynolds number simulations since KH rolls cannot sustain their lateral structure. Snapshots of the logarithmic kinetic energy dissipation field are shown in Fig. 6. In the laminar cases, ε is higher at the nose of the gravity currents where ε is of magnitude $O(10^{-7})$. Results indicate that the dissipation rate is lower in the KH rolls than in the rest of the shear region in the Re = 1000 case. The high dissipation field is visible as a strain region between two KH rolls. As the Re is increased, the magnitude of ε is reduced to $O(10^{-10})$ at the interface between the two layers.

Time evolutions of the relative background potential energy are provided in Fig. 7 for different Reynolds numbers. In the lowest Reynolds number experiment (Re = 125), the kinetic energy dissipates very quickly since the flow is laminar (panel 6(a)). This leads to a smearing of the interface between the upper and the lower layers. Thus, the relative background potential energy increases rapidly in the Re = 125 simulation (gray line in Fig. 7). In the Re = 500 simulation, the mixing is reduced significantly since the kinetic energy dissipation is decreased. For the rest of the experiments, RBPE increases as the Reynolds number increases after Re = 1000. Initial 2D mixing due to KH vortices occurs before $t/\tau^* \approx 2.5$. After that time, a vigorous amount of mixing occurs due to 3D turbulence since the flow has sufficiently large Reynolds number.

Next, mixing efficiency values will be compared for different Re simulations. In addition to (9), Prastowo et al. (2008) proposed a new definition of mixing efficiency, which can be written in the case of complete run-down of the exchange flow to a final state of no motion, as

$$\mu_2 = \frac{PE_f - BPE_i}{PE_i - BPE_i} = \frac{PE_f - BPE_i}{APE_i} \tag{12}$$

where PE_f is the final potential energy (note that subscripts i and f imply initial and final conditions, respectively). Eq. (12) defines the mixing efficiency as the ratio of how much irreversible mixing occurs at the expense of available potential energy of the system. Laboratory experiments performed by Prastowo et al. (2008) and Prastowo et al. (2009) showed that the mixing efficiency in two-layer exchange flows with constrictions saturates around $\mu_2 \approx 0.11 \pm 0.01$. In the lock-exchange flow, the initial background potential energy is $BPE_i = PE_i/2$ where PE_i is the initial potential energy. Thus, the initial available potential energy of the system is also equal to $APE_i = PE - BPE = PE_i/2$. Therefore, an analytical formulation can be derived for Eq. (12) using the final state of the lock-exchange flow. The flow is at rest and well-stratified, so $PE_f = BPE_f$. If both the numerator and denominator are divided by BPE_i, an analytical value for mixing efficiency is obtained as

$$\mu_2^{an} = \frac{(BPE_f - BPE_i)/BPE_i}{APE_i/BPE_i}. \tag{13}$$

Özgökmen et al. (2009) showed that in the final mixing state $(BPE_f - BPE_i)/BPE_i = 1/9$ and initially $APE_i = BPE_i$, thus $\mu_2^{an} = 1/9 \approx 0.111$ which is consistent with laboratory observations. Arneborg (2002) also suggested a similar analytical function for

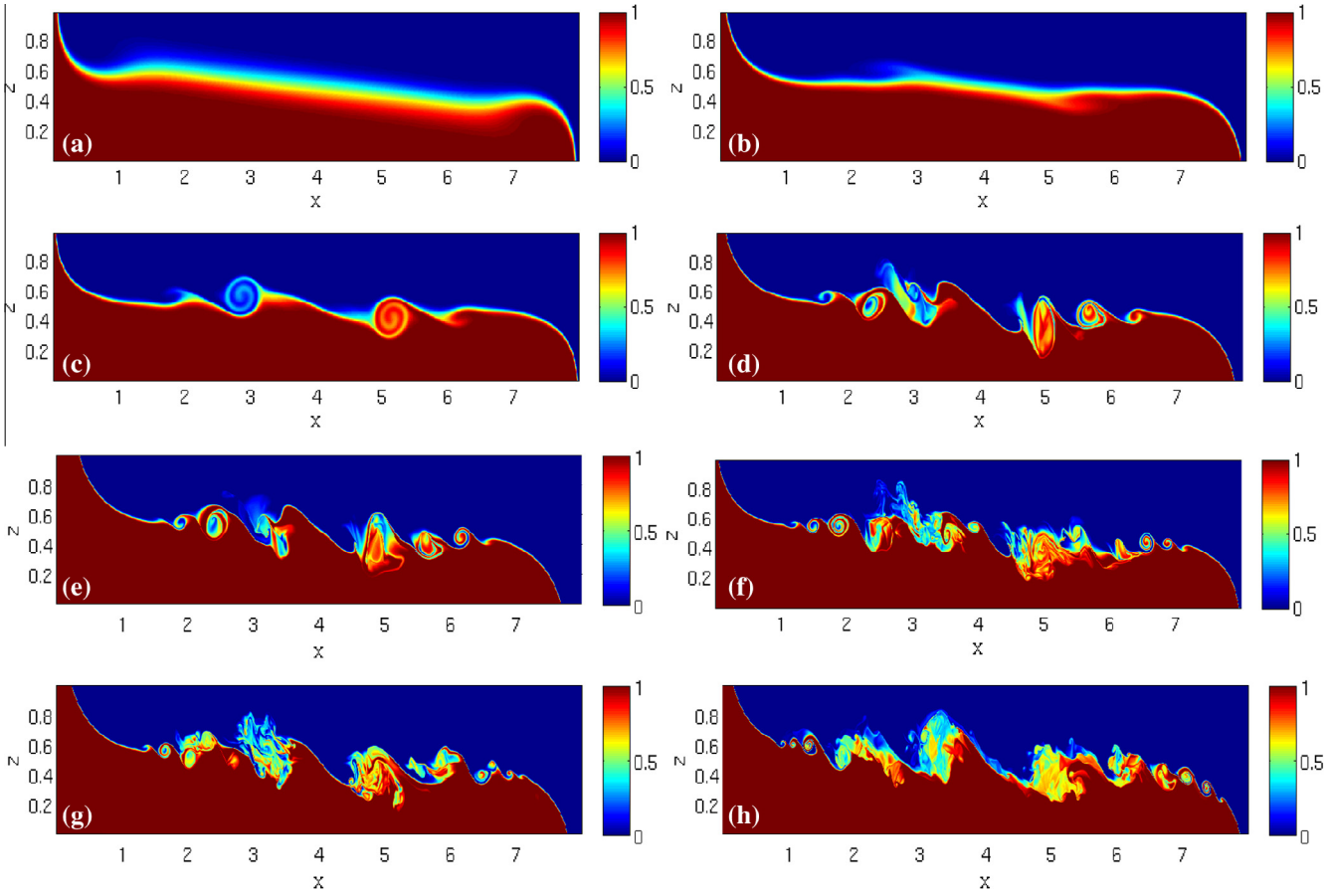

Fig. 5. Snapshots of density field at $y = 0.25$ and at $\tau = 0.6125$ for (a) Re = 125, (b) Re = 500, (c) Re = 1000, (d) Re = 2500, (e) Re = 3500, (f) Re = 5000, (g) Re = 6000, (h) Re = 10,000.

mixing efficiency. He proposed a mixing efficiency of 0.11 should be used in the oceans, lakes and fjords.

The mixing efficiency values computed using Eqs. (9) and (12) are shown in Fig. 8 as a function of Reynolds number. In the previous method (Eq. (9)), the cumulative mixing efficiency (μ_1) increases monotonically from Re = 125 to Re = 1000 and then μ_1 saturates around 0.1 for Re = 2500, Re = 3500, Re = 5000, Re = 6000 and Re = 10,000 (black circles in Fig. 8). The new method to compute efficiency (μ_2) is qualitatively similar to that previously applied. As the Reynolds number increases, so does the mixing efficiency until $\mathrm{Re} = 10^3$, and it then saturates around 0.12 ± 0.02. There are some quantitative differences between the two methods. The second method results in values of mixing efficiency that are lower than the first for low and high Reynolds numbers. However, at intermediate Re number cases, an opposite behavior can be observed. Note that the simulations are not integrated to full no-motion state. Thus, the definition of the BPE_f might not be accurate and this might be an explanation of the differences between the two mixing efficiency values. Because of computational limitations, higher Re numbers and/or longer simulations were not feasible. Note that over 3.5 billion grid points are employed for the $\mathrm{Re} = 10^4$ case. The key result in this study is that all mixing efficiency values computed here are lower than 0.166. This is consistent with the values of μ measured in Prastowo et al. (2008). However, it has to be mentioned that Prastowo et al. (2008) found that saturation of mixing efficiency occured after Re = 50,000 since their definition of Reynolds number is slightly different than ours. They used the constriction length scale in their Reynolds number and they also used higher density ratios in the lab experiments.

4. Discussion and concluding remarks

Mixing of fluids is a great interest for understanding geophysical fluid flows, especially in the ocean where mixing of water masses maintains the large scale vertical ocean stratification. One of the open questions in oceanography concerns the energetics of the overturning circulation. There is an ongoing debate regarding the magnitude of mixing required to sustain this circulation (Hughes et al., 2009). Resolving this issue is outside the scope of this paper. Here, energetics and the mixing efficiencies of high Reynolds number turbulent gravity currents are investigated. We conducted idealized lock-exchange flow experiments using at different Reynolds numbers.

Idealized laboratory and numerical experiments always have limitations compared to realistic oceanic flows. For instance, when we integrated the simulations long enough, the sloshing effect due to the solid walls became an important process. This sloshing effect is not important in some overflows (e.g. the Mediterranean overflow) but it can be crucial in others (e.g. the Red Sea overflow). Ilıcak et al. (2009) showed that in the Bosphorus Strait, the exchange flow interacts with the lateral boundaries when the gravity current flows in the s-shaped channel. Nevertheless, the 3D lock-exchange problem is a very good test case since it contains different turbulent processes at the same time.

The main results are the following. Firstly, the effect of spatial resolution is investigated at a relatively high Reynolds number of 3500. Four different simulations are carried out with different resolutions. Our results indicate that resolving Kolmogorov scale is sufficient, and resolving the Batchelor scale is not necessary in terms of evolution of relative background potential energy, tracer

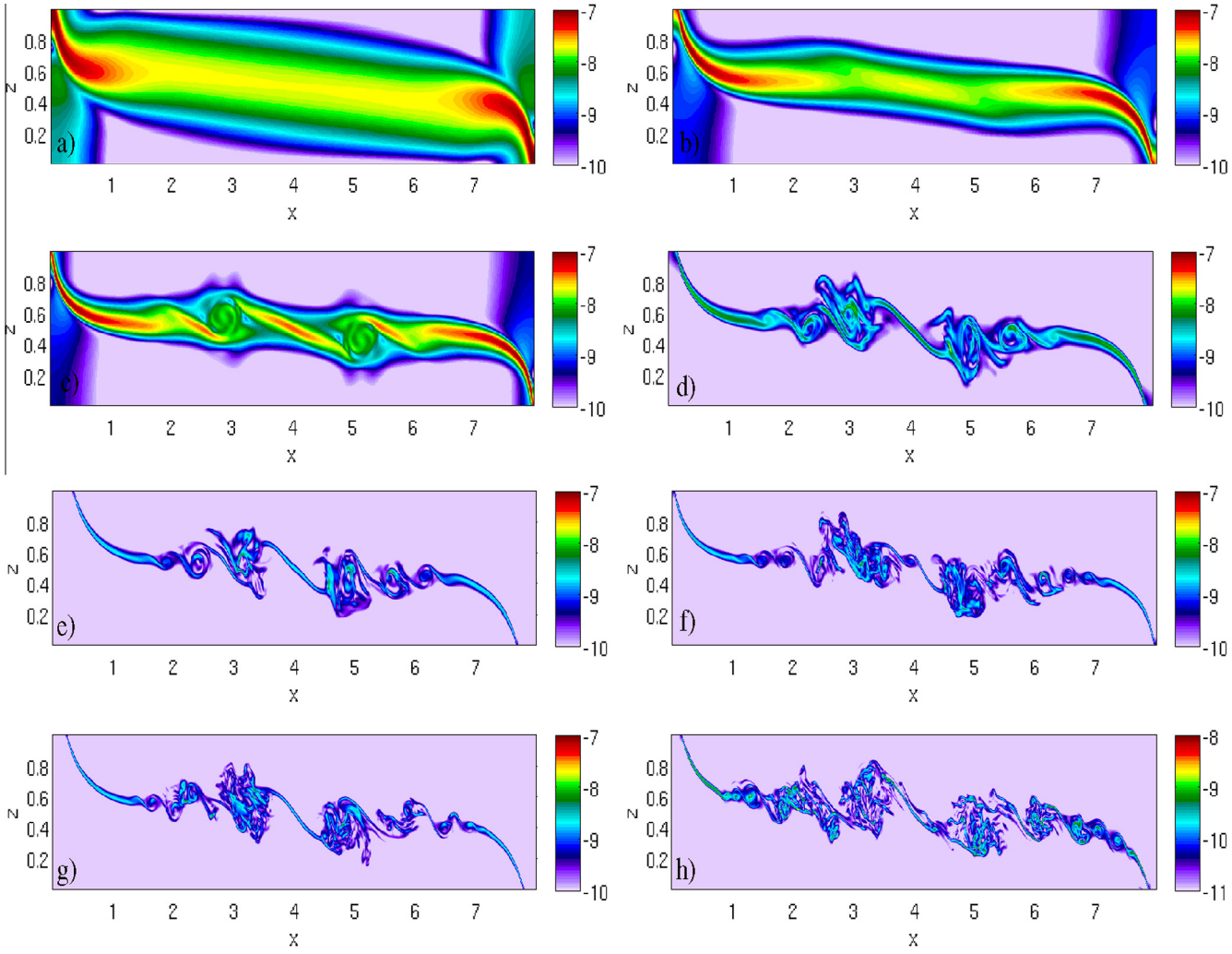

Fig. 6. Snapshots of logarithmic dissipation field at $y = 0.25$ and at $\tau = 0.6125$ for (a) Re = 125, (b) Re = 500, (c) Re = 1000, (d) Re = 2500, (e) Re = 3500, (f) Re = 5000, (g) Re = 6000, (h) Re = 10,000.

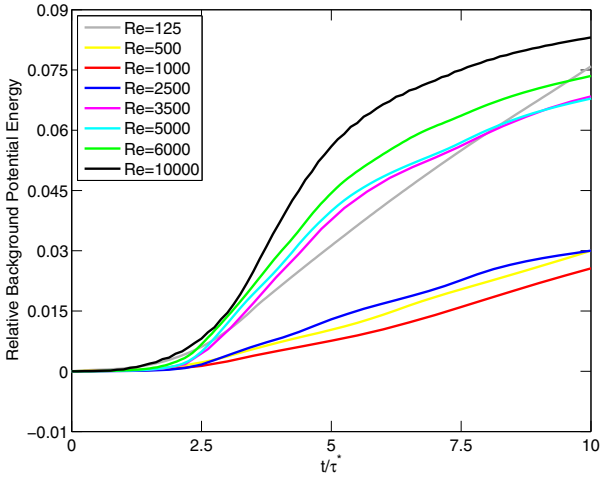

Fig. 7. Relative background potential energy vs. time for different Reynolds number simulations.

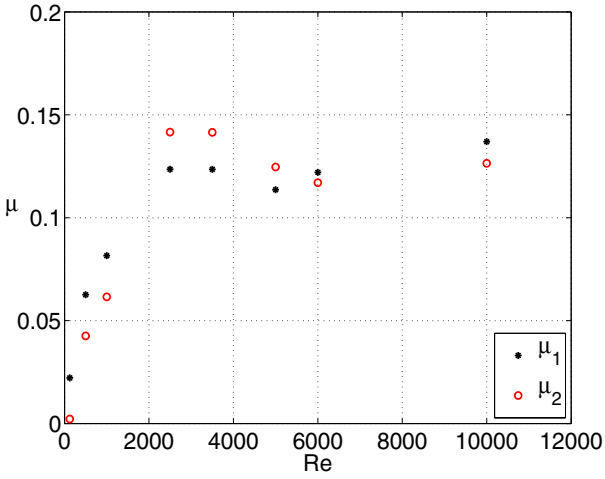

Fig. 8. Mixing efficiency values computed using different definitions for different Reynolds number simulations.

variance and kinetic energy dissipation fields. It is important to emphasize that the models are not converged in pure numerical sense, but they do so in the sense of metrics defined above. Coarse resolution simulations overestimate the total amount of mixing. Next, eight simulations of different Reynolds numbers are employed at $Ri = 2$ in the lock-exchange test case. These simulations are for $\mathrm{Re} = 125,\ 500,\ 1000,\ 2500,\ 3500,\ 5000,\ 6000$ and finally $\mathrm{Re} = 10,000$. Two different methods are employed to compute the mixing efficiency (Eqs. (9) and (12)). There are two different regimes in the behavior of mixing efficiency. It increases linearly with the Reynolds number provided Re is small (less than 2000), and saturates at 0.12 ± 0.02 for moderate and higher Reynolds numbers. A high amount of momentum dissipation and mixing occurs when KH rolls break down. The mixing efficiency values are consistent with Prastowo et al. (2008), who obtained approximately $\mu = 0.11 \pm 0.01$ in laboratory studies of high Reynolds number buoyancy-driven exchange flow in a channel with a constriction.

The results provided here suggest that the bulk mixing efficiency in buoyancy-shear driven flows (such as gravity currents) might saturate around 0.12 at high Reynolds number which is a typical characteristic of geophysical flows. However in the oceans, internal gravity waves and lee waves are some of the crucial processes that sustain the interior stratification. Coarse resolution ocean general circulation models cannot represent the mixing associated with these processes and so they employ various diapycnal mixing parameterizations, often assuming the same mixing efficiency of 0.2 for all processes. Examples of these parameterizations are: internal wave parameterizations and gravity current bottom boundary layer mixing parameterizations (Simmons et al., 2004; Legg et al., 2006). However, it is known that Kelvin–Helmholtz rolls, observed in gravity currents, are also one of the main mechanisms of mixing in breaking internal waves and lee waves (Troy and Koseff, 2005; Abe and Nakamura, 2013). Thus, mixing efficiency might be smaller than the traditional value attributed to these processes. Note that the oceanography community uses the flux coefficient Γ defined by Osborn (1980) as the canonical value of mixing efficiency in their parameterizations. However, as previous studies suggest mixing efficiency should be defined as $\mu = \Gamma/(1+\Gamma)$ which leads to $\mu \approx 0.166$ which is still higher than values found in here.

If the mixing efficiency is less than 0.2 in some cases in the ocean, this means that ocean general circulation models are missing a key component of the energy budget (Arneborg, 2002). This might be diapycnal mixing due to mesoscale eddies (Nikurashin et al., 2013), open ocean deep water convection, double diffusive process or some other ocean physical processes. Although more investigation is required to make a definitive conclusion, present numerical results indicate that the traditional assumption of a constant value for the efficiency of mixing for all processes is an over-simplification.

Acknowledgment

We thank Dr. Ilker Fer, Dr. Marcello G. Magaldi and Dr. Martin P. King for their help improving language of the manuscript. We also thank three anonymous reviewers for their constructive criticism.

References

Abe, S., Nakamura, T., 2013. Processes of breaking of large-amplitude unsteady lee waves leading to turbulence. J. Geophys. Res. Oceans 118, 316–331.
Arneborg, L., 2002. Mixing efficiencies in patchy turbulence. J. Phys. Oceanogr. 32, 1496–1506.
Benjamin, T.B., 1968. Gravity currents and related phenomena. J. Fluid Mech. 31, 209–248.
Caulfield, C.P., Peltier, W.R., 2000. The anatomy of the mixing transition in homogeneous and stratified free shear layers. J. Fluid Mech. 413, 1–47.
Cushman-Roisin, B., Beckers, J.M., 2011. Introduction to Geophysical Fluid Dynamics: Physical and Numerical Aspects. Academic Press.
Dunne, J.P., John, J.G., Hallberg, R.W., Griffies, S.M., Shevliakova, E.N., Stouffer, R.J., Krasting, J.P., Sentman, L.A., Milly, P.C.D., Malyshev, S.L., Adcroft, A.J., Cooke, W., Dunne, K.A., Harrison, M.J., Levy, H., Samuels, B.L., Spelman, M., Winton, M., Wittenberg, A.T., Phillips, P.J., Zadeh, N., 2012. GFDLs ESM2 global coupled climate-carbon earth system models part I: physical formulation and baseline simulation characteristics. J. Climate 25, 6646–6665.
Gayen, B., Griffiths, R.W., Hughes, G.O., Saenz, J.A., 2013. Energetics of horizontal convection. J. Fluid Mech. 716, 716.
Gregg, M.C., Ozsoy, E., 2002. Flow, water mass changes, and hydraulics in the Bosphorus – art. no. 3016. J. Geophys. Res.-Oceans 107 (C3), 3016.
Hartel, C., Kleiser, L., Michaud, M., Stein, C.F., 1997. A direct numerical simulation approach to the study of intrusion fronts. J. Eng. Math. 32, 103–120.
Hughes, G.O., Hogg, A.M., Griffiths, R.W., 2009. Available potential energy and irreversible mixing in the meridional overturning circulation. J. Phys. Oceanogr. 39, 3130.
Hult, E.L., Troy, C.D., Koseff, J.R., 2011. The mixing efficiency of interfacial waves breaking at a ridge: 1. Overall mixing efficiency. J. Geophys. Res. 116, 2003.
Ilcak, M., Vallis, G.K., 2012. Simulations and scaling of horizontal convection. Tellus A 64, 183377.
Ilcak, M., Özgökmen, T.M., Peters, H., Baumert, H.Z., Iskandarani, M., 2008. Performance of two-equation turbulence closures in three-dimensional simulations of the Red Sea overflow. Ocean Modell. 24, 122–139.
Ilıcak, M., Armi, L., 2010. Comparison between a non-hydrostatic numerical model and analytic theory for the two-layer exchange flows. Ocean Modell. 35, 264–269.
Ilıcak, M., Özgökmen, T.M., Özsoy, E., Fischer, P.F., 2009. Non-hydrostatic modeling of exchange flows across complex geometries. Ocean Modell. 29, 159–175.
Ilıcak, M., Adcroft, A.J., Griffies, S.M., Hallberg, R.W., 2012. Spurious dianeutral mixing and the role of momentum closure. Ocean Modell. 45, 37–58.
Klaassen, G.P., Peltier, W.R., 1991. The influence of stratification on secondary instability in free shear layers. J. Fluid Mech. 227, 71–106.
Klymak, J., Legg, S., Alford, M.H., Buijsman, M.C., Pinkel, R., Nash, J.D., 2012. The direct breaking of internal waves at steep topography. Oceanography 25, 150–159.
Legg, S., Hallberg, R.W., Girton, J.B., 2006. Comparison of entrainment in overflows simulated by z-coordinate, isopycnal and non-hydrostatic models. Ocean Modell. 11, 69–97.
Marshall, J., Adcroft, A., Hill, C., Perelman, L., Heisey, C., 1997. A finite-volume, incompressible Navier Stokes model for studies of the ocean on parallel computers. J. Geophys. Res. 102, 5753–5766.
Mashayek, A., Peltier, W.R., 2011. Three-dimensionalization of the stratified mixing layer at high Reynolds number. Phys. Fluids 23 (11), 111701.
Mashayek, A., Caulfield, C.P., Peltier, W.R., 2013. Time-dependent, non-monotonic mixing in stratified turbulent shear flows: implications for oceanographic estimates of buoyancy flux. J. Fluid Mech. 736, 570–593.
Moum, J.N., 1996. Energy-containing scales of turbulence in the ocean thermocline. J. Geophys. Res. 101, 14095–14109.
Munk, A., 1966. Abyssal recipes. Deep-Sea Res. 13, 707–730.
Nikurashin, M., Vallis, G.K., Adcroft, A., 2013. Routes to energy dissipation for geostrophic flows in the Southern Ocean. Nat. Geosci. 6, 48–51.
Osborn, T.R., 1980. Estimates of the local rate of vertical diffusion from dissipation measurements. J. Phys. Oceanogr. 10, 83–89.
Özgökmen, T.M., Iliescu, T., Fischer, P.F., 2009. Large eddy simulation of stratified mixing in a three-dimensional lock-exchange system. Ocean Modell. 26, 134–155.
Özgökmen, T.M., Iliescu, T., Fischer, P.F., 2009. Reynolds number dependence of mixing in a lock-exchange system from direct numerical and large eddy simulations. Ocean Modell. 30, 190–206.
Peltier, W.R., Caulfield, C.P., 2003. Mixing efficiency in stratified shear flows. Annu. Rev. Fluid Mech. 35, 135–167.
Peters, H., Johns, W.E., 2005. Mixing and entrainment in the red sea outflow plume. Part ii: turbulence characteristics. J. Phys. Oceanogr. 35, 584–600.
Peters, H., Gregg, M.C., Sanford, T.B., 1995. Detail and scaling of turbulent overturns in the pacific equatorial undercurrent. J. Geophys. Res. 100, 18349–18368.
Pham, H.T., Sarkar, S., 2010. Internal waves and turbulence in a stable stratified jet. J. Fluid Mech. 648, 297.
Pope, S.B., 2000. Turbulent Flows. Cambridge University Press.
Prastowo, T., Griffiths, R.W., Hughes, G.O., Hogg, A.M., 2008. Mixing efficiency in controlled exchange flows. J. Fluid Mech. 600, 235–244.
Prastowo, T., Griffiths, R.W., Hughes, G.O., Hogg, A.M., 2009. Effects of topography on the cumulative mixing efficiency in exchange flows. J. Geophys. Res. 114, 8008.
Ruddick, B., Walsh, D., Oakey, N., 1997. Variations in apparent mixing efficiency in the north atlantic central water. J. Phys. Oceanogr. 27, 2589–2605.
Sandström, J.W., 1908. Dynamische versuche mit meerwasser. Ann. Hydrodyn. Mar. Meteorol. 36, 4–48.
Scotti, A., White, B., 2011. Is horizontal convection really non-turbulent? Geophys. Res. Lett. 38, 21609.
Simmons, H.L., Jayne, S.R., St.Laurent, L.C., Weaver, A.J., 2004. Tidally driven mixing in a numerical model of the ocean general circulation. Ocean Modell. 6, 245–263.

Smyth, W.D., Moum, J.N., Caldwell, D.R., 2001. The efficiency of mixing in turbulent patches: inferences from direct simulations and microstructure observations. J. Phys. Oceanogr. 31, 1969–1992.
Tailleux, R., 2009. Understanding mixing efficiency in the oceans: do the nonlinearities of the equation of state matter? Ocean Sci. 5, 271–283.
Troy, C.D., Koseff, J.R., 2005. The instability and breaking of long internal waves. J. Fluid Mech. 543, 107–136.
Winters, K.B., Young, W.R., 2009. Available potential energy and buoyancy variance in horizontal convection. J. Fluid Mech. 629, 221–230.
Winters, K.B., Lombard, P.N., Riley, J.J., D'Asaro, E.A., 1995. Available potential energy and mixing in density-stratified fluids. J. Fluid Mech. 289, 115–128.
Wunsch, C., Ferrari, R., 2004. Vertical mixing, energy, and the general circulation of the ocean. Annu. Rev. Fluid Mech. 36, 281–314.